Article

Not peer-reviewed version

Dipolar Brush Polymers: A Numerical Study of the Force Exerted onto a Penetrating Colloidal Particle Under an External Field

A. Fuster-Aparisi , Antonio Cerrato , Josep Batle , Joan Josep Cerdà *

Posted Date: 17 December 2024

doi: 10.20944/preprints202412.1431.v1

Keywords: Dipolar brushes; magnetic brushes; colloids; numerical simulations; Langevin Dynamics

 doi:10.20944/preprints202412.1431.v1

Article

Dipolar Brush Polymers: A Numerical Study of the Force Exerted onto a Penetrating Colloidal Particle Under an External Field

A. Fuster-Aparisi [1], Antonio Cerrato [2], Josep Batle [1] and Joan Josep Cerdà [1,*]

[1] Departamento de Física UIB i Institut d'Aplicacions Computacionals de Codi Comunitari (IAC3), Campus UIB, E-07122 Palma de Mallorca, Spain
[2] Departamento de Ingeniería de la Construcción y Proyectos de Ingeniería. Escuela Técnica Superior de Ingeniería, Universidad de Sevilla, Camino de los Descubrimientos, 41092 Sevilla, Spain
[3] Computational and Soft Matter Physics, Faculty of Physics, University of Vienna, 1090 Vienna, Austria
* Correspondence: jj.cerda@uib.cat; Tel.: +34-971-172332

Abstract: Langevin Dynamics numerical simulations have been used to compute the force profiles that dipolar polymer brushes exert onto a penetrating colloidal particle. It has been observed that force profiles are strongly influenced by external applied fields: a force barrier at large distances from the grafting surface appears, and at shorter distances a region with lower repulsive forces develops. Furthermore, for a right combination of polymer grafting density, polymer chain length and strength of the external field, it is possible to observe in such intermediate region the existence of net attractive forces onto the penetrating particle, and the emergence of a stationary point. The existence of these regions of low repulsive or net attractive forces inside the dipolar brushes, as well as their dependence on the different parameters of the system can be qualitatively reasoned in terms of a competition between steric repulsion forces and Kelvin forces arising from the dipolar mismatch between different regions of the system. The possibility to tune force profile features such as force barriers and stationary points via an external field paves the way for many potential surface-particle related applications.

Keywords: dipolar brushes; magnetic brushes; colloids; numerical simulations; Langevin dynamics

1. Introduction

Polymer brushes are soft-matter systems in which polymer chains are anchored or attached by one of their ends to a surface. Advances in chemistry synthesis have allowed to create many different types of polymer brushes and research on the topic is still very active [1–14]. The understanding of their properties via experiments [15–24], theory [18,20,25–32,32–39], numerical simulations [28,30–32,40–46], Self Consistent Field approaches [47–50], as well as the optimization and design of new applications [9,51–71] involving such systems are also very prominent areas of research in the field of polymer science.

Within the field of polymer brushes, a topic that has raised considerable attention is the study of the force exerted by a brush onto a particle. The case of neutral polymer brushes has drawn a lot of attention in the past: a full Self Consistent Field Theory (SCFT) suitable for particles of small radii was developed by Kim and Matsen [72]: within such framework the free energy penalty exerted onto a spherical particle by a neutral polymer brush was studied, and the suitability of the strong-stretching theory of Milner, Witten and Cates, as well as the Derjaguin approach were analysed. SCFT were also used by Egorov et al [73] and Lian et al. [74] in order to study how solvent (good or bad solvent) influences the effective interactions of nanoparticles in polymer brushes. On the other hand the interaction of nanoparticles with polymers brushes grafted inside porous substrates in both good and bad solvents was studied by Santo et al. [75]. Density functional theory (DFT) has also been used in predicting polymeric forces for antifouling applications [76].

In addition to SCFT and DFT, numerical simulations have also been widely used to study the force between a brush and a colloidal particle. For instance Milchev et al. [77] studied it using a

 doi:10.20944/preprints202412.1431.v1

coarse-grained off-lattice bead spring model and Montecarlo Simulations, and two years later Ermilov et al. [78] also reviewed it. Dissipative Particle Dynamics simulations where also used by Milchev et al. [79] to study the case of neutral polymer brushes with nanoinclusions under shear flow. The inclusion free energy of nanoparticles in polymer brushes was also studied in detail using Molecular Dynamics by Merlitz et al. [80]. The absortion and the force exerted by repulsive and attractive brushes onto a spherical particle were also studied by Zhang et al more than a decade ago [81] using Brownian Dynamics.

More recently, the insertion forces for particles of different geometry into neutral polymer brushes have been studied by Beer et al. [82] and Gao et al [83], and more advanced SCFT theories have been applied to the study of the interaction of inclusions with neutral polymeric brushes [84,85]. In the case of Spencer et al. [84] the study also included the case of brushes with mobile grafted chains. For systems in which the grafting surface is permeable to the fluid, the interaction of a particle and a neutral polymer brush has been thoroughly studied by Offner et al. [86].

The study of particles inside brushes has not been only limited to the study of the force profiles exerted by the brushes, transport theory of colloids across the polymer brushes has also been reviewed by Laktionov et al. [87]. In addition, molecular dynamics simulations and Asakura-Oosawa models have been used to address the depletion induced in proteins embedded in polymer brushes [88], and a theory to account for the interaction of polymer brushes with antimicrobial peptides has been developed [89]. It is also worth to mention that the controlled adsorption via pH of nanoparticles on polyelectrolyte brushes has also been recently addressed by Astier et al. [90]. Very recently, in the case of polyelectrolyte brushes, Popova et al. [91] using mean-field Poisson-Boltzmann approximation have shown that a nanoparticle uptake by the brush exists when the interaction of the brush with the particle promotes changes in the ionization state of the weak cationic and anionic groups in the surface of the nanoparticle.

Another topic of high interest in the field of polymer brushes are dipolar brushes, within such sub-field, a case that has recently received considerable attention are the supramolecular polymeric brushes in which magnetic colloidal particles play the same role than monomers in a traditional chemical polymer. These systems constitute a particular type of magnetoresponsive thin film surfaces [92,93] for which several synthesis pathways have already been developed [94–104]. Superparamagnetic and paramagnetic brushes have been used to design magnetoresponsive nanoscaled actuators [94] analogous to polymer responsive brushes [105] and micro-metric cilia arrays [106–108]. The approach followed has mostly consisted in modelling the filaments as elastic rods in which the direction and strength of the magnetic dipoles are induced by the oscillating external field. More recently, the study of magnetic brushes made of fully magnetic ferromagnetic filaments has also been addressed [98,109–115].

Most of the previous studies about magnetic brushes have focussed on brushes containing a single class of filaments fully magnetic where only magnetic interactions among dipoles and steric repulsion among the core of colloids is present [98,109–113]. The only exceptions are the works of Cerdà et al. [114,115] where the role of an additional short-range attractive interaction among colloidal particles and the possibility that magnetic filaments may only be partially magnetic have been considered. To our best knowledge, no study has focused so far on the interaction of these magnetic brushes with non-magnetic particles.

The interest in these magnetic or dipolar brushes is driven by their promising role in technological applications in the areas of: actuators and mixers [95,106,116,117], dynamical absorbers [118], micromechanical sensors [119], non-permanent photonic crystals [120], diffraction gratings [121], or medicine [122,123], to mention just a few [124]. Filaments that react to external magnetic fields have several advantages with respect to the more traditional polymer and polyelectrolyte brushes, which are more constrained in their responsivity to external fields: changes in pH or the electric field have a strong and complex impact not only on the polymer brush but also on most of the soft matter substances. For these reasons, the research of magnetic brushes is evolving into a very promising field.

 doi:10.20944/preprints202412.1431.v1

In this work, we aim at the study of flat dipolar brushes interacting with a colloidal non-dipolar particle that penetrates into the brush. We want to expand the current knowledge about dipolar brushes by studying the dependence of the force profile observed on several parameters: the radius of the penetrating particle, the fraction of dipolar particles present in the brush, the strength of the external imposed field, and the grafting density of the brush. In this study, it will be shown that for some range of brush-particle parameters and field strengths there exists an attractive zone for the colloidal particle inside the brush. In what follows we will always exemplify our study via magnetic colloidal systems, but it should be noticed that all results derived in this work using magnetic dipoles and magnetic external fields can be easily mapped to the case of electric dipoles and external electric fields as all the interactions have the same structure in both cases except for a constant pre-factor.

The present manuscript is organised in the following way. In the next section, the numerical model and the details of the simulations are described. The main findings are provided in Section 3. Finally, the summary of our main results is provided in Section 4.

2. Numerical Method

The dipolar brushes are modelled as a regular squared lattice array of $N_c \times N_c$ spring-bead chains made of N monomers per chain, all them grafted by one of their ends at the plane x-y at $z = 0$. The brush is placed into a cubic box of edge L_e where periodic boundary conditions along x-y directions are allowed, and a large non-dipolar colloidal particle of radius R_e is placed with its centre at position $(L_e/2, L_e/2, z_{eo})$, where z_{eo} is larger than the length of a fully extended chain, see Figure 1a. In our simulations, several types of chain sequences are tested in order to understand how the brush structure depends on the number of dipolar monomers present in the chains. In a given simulation all chains have the N_{dip} dipolar monomers equispaced along the chain sequence where the free-end monomer always carries a dipole (see an scheme in Figure 1b). All chain beads, dipolar and non-dipolar are assumed to be spheres of diameter σ_e and mass m_e.

Subindex e has been used to denote the experimental values of the physical quantities we use. Instead, in the numerical simulations reduced units are used. For instance, all length scales in the simulations are measured in units of the bead diameter and therefore the corresponding reduced value of any experimental length l_e is $l = l_e/\sigma_e$. In this way $R = R_e/\sigma_e$, $L = L_e/\sigma_e$, $z_o = z_{eo}/\sigma_e$ and due to the previous definition, the diameter of all chain beads or monomers is set to $\sigma = 1$.

In order to link the monomers that form a chain, we use a finite extension non-linear elastic (FENE) potential [125] among adjacent monomers in the chain sequence,

$$U_s(r) = -\frac{1}{2} K_s \Delta r_{max}^2 \ln\left[1 - \left(\frac{r - r_0}{\Delta r_{max}}\right)^2\right], \tag{1}$$

where the constants of the potential are set to $r_0 = \sigma$, $\Delta r = 1.5\sigma$ and $K_s = 15$.

All short range isotropic interactions between monomers in the present model are of Lennard-Jones (LJ) type. Thus the monomers interact among themselves according to the potential

$$U_{att}(r) = V_{tsLJ}(r, \sigma, 1, r_{cut} = 2^{1/6}\,\sigma) + V_{tsLJ}(r, \sigma, \varepsilon, r_{cut} = 2.5\,\sigma) \tag{2}$$

where r is the distance between the centres of the monomers i and j, *i.e.* $r = |\boldsymbol{r}_i - \boldsymbol{r}_j|$, and V_{tsLJ} is a truncated-shifted Lennard-Jones potential [126],

$$V_{tsLJ}(r, d, U_o, r_cut) = \begin{cases} U_{LJ}(r) - U_{LJ}(r_{\rm cut}), & \text{for } r < r_{\rm cut} \\ 0, & \text{for } r \geq r_{\rm cut} \end{cases}, \tag{3}$$

where $U_{LJ}(r) = 4U_o[(d/r)^{12} - (d/r)^6]$. First truncated-shifted LJ (cut-off $r_{cut} = 2^{1/6}\sigma$) in Equation (2) stands for the core repulsive part and second truncated-shifted LJ ($r_{cut} = 2.5\sigma$) for the attractive part. The reason to model the short-range part of the beads interaction with two truncated-shifted potentials

 doi:10.20944/preprints202412.1431.v1

and not just a simple LJ is to always have roughly the same repulsive core interaction independently of the value of attractive depth well ε. This allows a much easier comparison between different values of ε and the effective particle size is kept roughly similar in all cases.

In the simulations, all the energies are given in units of the experimental well depth ε_e between two monomers. Thus the expression to map a physical energy value U_e to its counterpart in the reduced unit system U is $U = U_e/\varepsilon_e$. In the same way Boltzmann constant is chosen to be $k = 1$ in reduced units, and therefore the reduced temperature is $T = k_e T_e/\varepsilon_e$.

The interaction between any monomer and the penetrating colloidal particle of radius R is modelled via a purely repulsive potential

$$U_{rep}(r) = V_{tsLJ}(r, R + \sigma/2, 1, r_{cut} = 2^{1/6}\,(R + \sigma/2)) \tag{4}$$

In addition all the chain monomers present in the system exhibit an steric repulsion with the grafting surface located at the x–y plane that is modelled using a standard $9-3$ WCA potential:

$$V_{wall} = \begin{cases} U_{wall}(r) - U_{wall}(r_{\text{cut}}), & \text{for } r < r_{\text{cut}} \\ 0, & \text{for } r \geq r_{\text{cut}} \end{cases}, \tag{5}$$

where $U_{wall}(r) = [(\sigma/r)^9 - (\sigma/r)^3]$ and $r_{cut} = 3^{1/6}\sigma$ in this case. The grafted monomers of the chains are placed at $z = 3^{1/6}\sigma$, which corresponds to $V_{wall} = 0$. No repulsive interaction is set between the grafting surface and the penetrating particle as the particle is never at close contact with the surface, and we want to focus specificaly on the influence of the monomers of the brush on that particle.

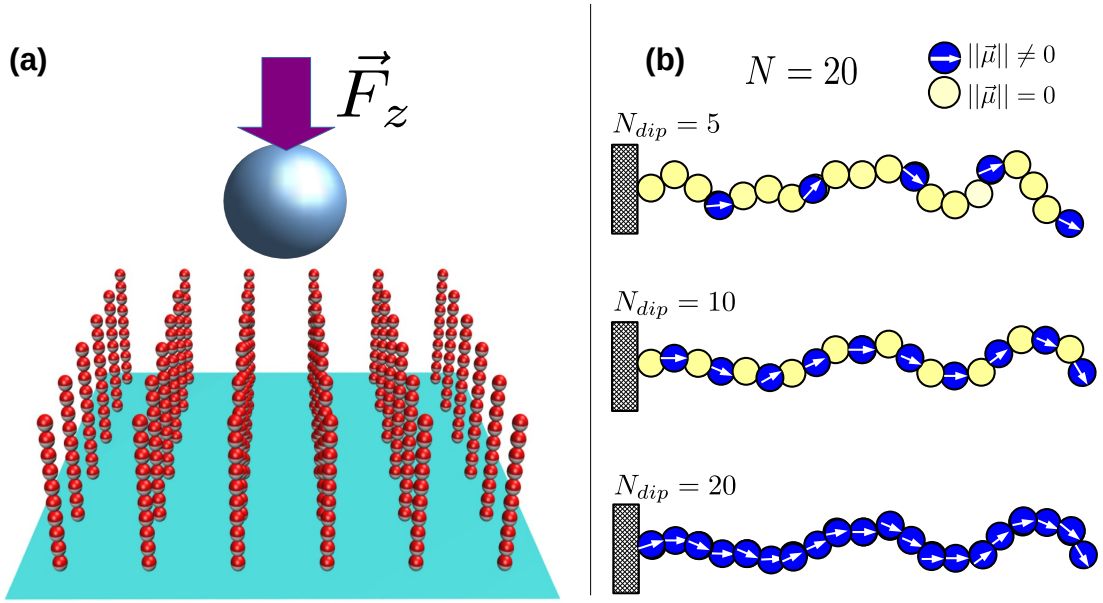

Figure 1. The figure (**a**) depicts an schematic view of the system under study, the figure (**b**) shows some of the chain dipolar sequences tested in this work, N_{dip} and N indicate the number of dipolar monomers and the total number of monomers per chain, respectively.

A point dipole $\boldsymbol{\mu}_e$ is assigned to each dipolar monomer, the dipoles are located at the centre of the monomers, and fixed within the particle body, so that its rotation is coupled to the rotation of the monomer. The modulus of the dipole moments in reduced units is calculated from the following

 doi:10.20944/preprints202412.1431.v1

relation: $\mu^2 = \mu_e^2/(\sigma_e^3\varepsilon_e)$, where $|\mu^2| = \mu$. There are two types of interactions related to the dipoles. The first one is the dipole-dipole interaction:

$$U_{\rm dip}(\boldsymbol{r}_{ij}, \boldsymbol{\mu}_i, \boldsymbol{\mu}_j) = \frac{\boldsymbol{\mu}_i \cdot \boldsymbol{\mu}_j}{r^3} - \frac{3[\boldsymbol{\mu}_i \cdot \boldsymbol{r}_{ij}][\boldsymbol{\mu}_j \cdot \boldsymbol{r}_{ij}]}{r^5}, \tag{6}$$

where $\boldsymbol{r}_{ij} = \boldsymbol{r}_i - \boldsymbol{r}_j$ is the displacement vector between particles i and j. In the case of magnetic colloidal polymer brushes, reasonable values of $\mu = |\boldsymbol{\mu}|$ depend in general on the composition and size of the nanoparticles, but in usual ferrofluids typically it does not exceed $\mu_e^2/(kT_e\sigma_e^3) \sim 10$. The long-range dipole-dipole interactions in this half-space geometry are calculated using a two fold step: first dipolar interactions are calculated using the standard P^3M algorithm (dP^3M) [127] that implicitly assumes periodic boundary conditions along all directions; secondly, a dipolar layer correction (DLC) [128] is applied which discounts the effect of the excess of infinite replicas added along the z direction in the first step of the calculation. The combined use of dP^3M and DLC methods allows a much faster calculation of the dipolar long-range interactions that the traditional two-dimensional dipolar Ewald summations [129] adapted to slit geometries: computer times scale with the total number of dipolar particles $N_d = N_c^2\, N_{dip}$ present in the system as $N_d \ln(N_d)$ and $N_d^{3/2}$ respectively. The level of accuracy of the algorithm for computing dipolar forces and torques is set in our simulations to $\delta \sim 10^{-4}$.

The dipoles are also allowed to interact with an external field $\boldsymbol{H}_e$. Its orientation will be kept fixed along the z-direction, so that in reduced units $\boldsymbol{H} = (0, 0, H)$, where $H = H_e\sqrt{\sigma_e^3/(\varepsilon_e)}$. Therefore, the Zeeman energy can be written as:

$$U_{\rm H}(\boldsymbol{H}, \{\boldsymbol{\mu}_i\}) = -\sum_{i=0}^{N} \boldsymbol{H} \cdot \boldsymbol{\mu}_i = -H \sum_{i=0}^{N} \mu_{z_i}. \tag{7}$$

The numerical simulations are performed using Langevin dynamics. In this approach, all the monomers (except the grafted monomers and the penetrating particle whose positions are not updated at each time step) are moved according to the translational and rotational Langevin equations of motion that, for a given particle i, are [130]:

$$M_i \frac{d\mathbf{v}_i}{dt} = \boldsymbol{F}_i - \Gamma_T \boldsymbol{v}_i + \boldsymbol{\xi}_i^T + \Gamma_T \dot{\gamma} z_i \hat{\boldsymbol{x}} \tag{8}$$

$$\boldsymbol{I}_i \cdot \frac{d\boldsymbol{\omega}_i}{dt} = \boldsymbol{\tau}_i - \Gamma_R \boldsymbol{\omega}_i + \boldsymbol{\xi}_i^R \tag{9}$$

where $\boldsymbol{F}_i$, and $\boldsymbol{\tau}_i$ are respectively the total force and torque acting on the particle i. Γ_T and Γ_R are the translational and rotational friction constants. The dipolar component of the torque, $\boldsymbol{\tau}_i^{(dip)}$, can be computed as

$$\boldsymbol{\tau}_i^{(dip)} = -\boldsymbol{\mu}_i \times \nabla_{\boldsymbol{\mu}_i}(U_{\rm dip} + U_{\rm H}). \tag{10}$$

M_i and $\boldsymbol{I}_i$ are the mass and the inertia tensor of the colloid, and $\boldsymbol{\xi}_i^T$ and $\boldsymbol{\xi}_i^R$ are Gaussian random forces and torques, each of zero mean value and satisfying the usual fluctuation-dissipation relations

$$\langle \xi_{i\alpha}^T(t)\xi_{j\beta}^T(t')\rangle = 2kT\Gamma_T\delta_{ij}\delta_{\alpha\beta}\delta(t-t'), \tag{11}$$

$$\langle \xi_{i\alpha}^R(t)\xi_{j\beta}^R(t')\rangle = 2kT\Gamma_R\delta_{ij}\delta_{\alpha\beta}\delta(t-t'), \tag{12}$$

where α and β denote x, y, z for translation and rotation in Cartesian coordinates. Equations of motion (8) and (9) are a reasonable approach as far as the size of particles is such that sedimentation forces are negligible. In the simulations, $t = t_e\sqrt{\varepsilon_e/(m_e\sigma_e^2)}$, where m_e is the real mass of the monomers; $F = F_e\sigma_e/\varepsilon_e$, and $\tau = \tau_e/\varepsilon_e$. For equilibrium simulations, the values of the mass, the inertia tensor, as well as friction constants Γ_T, and Γ_R are irrelevant because the same equilibrium state is reached independently of their value. Only the dynamics to attain such equilibrium state may show differences.

 doi:10.20944/preprints202412.1431.v1

For simplicity reasons, the particle mass of the monomers is chosen to be $m = 1$ and the inertia tensor is chosen to be the identity matrix in order to ensure isotropic rotations $\boldsymbol{I} = \mathbf{1}$. It has also been chosen $\Gamma_T = 1$ and $\Gamma_R = 3/4$ because these values have been observed to produce a conveniently fast relaxation to the stationary. The reduced time step is set to $\delta t = 0.0005$ in order to ensure a correct integration of the equations of motion.

Simulations are performed as follows: the grafted monomer of each polymer is placed at its assigned square lattice position, and the penetrating particle is placed at $(L/2, L/2, z_o)$. Then, the polymer chains or filaments are grown avoiding overlaps. Subsequently while the penetrating particle is kept fixed, the brush is warmed up at $T = 1$ for $2 \cdot 10^5$ integrations with the dipolar interaction turned off while the time step is slowly increased from $10^{-3}\delta t$ to $0.05\delta t$. Right after, dipolar interactions and external field are turned on. If simulation is performed at $T = 1$ a second warm-up stage, consisting of $5 \cdot 10^5$ integrations, is performed while gradually raising the time step from $10^{-1}\delta t$ to δt. For simulations at $T < 1$, an annealing process using a gradual time step increase from time step $10^{-1}\delta t$ to δt is performed: the temperature is varied from $T = 1$ to its final value by performing a set of five annealing cycles of 10^5 steps each. In all simulations, the chain is further equilibrated for a period of $10^6\ e^{1/T}\ \delta t$ in order to ensure that the chain has reached the thermodynamic equilibrium regime. Once equilibration process is completed, we start the approaching sequence of the penetrating particle: this particle is attempted to move closer to the grafting surface from z to $z - \Delta z$ via small steps of $\Delta z/100$. If in one of those descending steps the penetrating particle overlaps with a monomer, the penetrating particle returns to its previous position and a further integration of $100\ e^{1/T}\delta t$ is done before attempting again the descending step. This process is repeated till the centre of the penetrating particle is at $z - \Delta z$. At that moment the system is reequilibrated at the new distance between the brush and the penetrating particle for another period of $10^6\ e^{1/T}\ \delta t$. Subsequently, measures of the force exerted by the monomers onto the penetrating particle, which position is kept fixed during the whole stage of measurements, are registered at intervals of $100\ e^{1/T}\delta t$ for a period of $2 \cdot 10^6\ e^{1/T}\ \delta t$. The process of further descending into the brush, equilibration and measuring the force onto the penetrating particle is repeated iteratively until reaching the desired final distance of the centre of the brush to the grafting surface which always is larger than $R + \sigma$. To make sure that the results do not depend on the initial conditions and to improve statistics, we additionally average the forces for each set of sampled parameters over 3 independent runs. All simulations have been performed using the package ESPResSo [131].

3. Results and Discussion

In order to facilitate the comparison with other works in which dipolar brushes are studied, it is convenient to define a set of non-dimensional parameters. The first one is the strength ratio of the short-ranged attractive interaction to the dipolar interaction

$$\eta \equiv \frac{\varepsilon\sigma^3}{\mu^2}, \tag{13}$$

where the two monomers are considered to be at close contact, $r_{ij} = \sigma$, and with their dipoles oriented in a nose-tail conformation. Two dipoles i and j are said to be in a nose-tail conformation when $\boldsymbol{\mu}_i \cdot \boldsymbol{\mu}_j = \mu^2$, and $\boldsymbol{\mu}_i \cdot \boldsymbol{r}_{ij} = \boldsymbol{\mu}_j \cdot \boldsymbol{r}_{ij} = \pm\mu\, r_{ij}$. The nose-tail alignment is the conformation that minimises the dipolar energy in eq.6. In this study we focus on two different values of this parameter: $\eta = 0$ that corresponds to a dipolar brush in a good solvent, and $\eta = 0.05$ for a brush in a bad solvent.

A second parameter of widespread use is the dipolar coupling parameter,

$$\lambda \equiv \frac{\mu^2}{kT\sigma^3}, \tag{14}$$

 doi:10.20944/preprints202412.1431.v1

that measures the relative strength of the dipolar interaction (same conditions as in the definition of η) to the thermal energy. In this work we fix $\lambda = 10$. A third parameter of interest when an external field is applied is the Langevin parameter,

$$\alpha \equiv \frac{\boldsymbol{\mu} \cdot \boldsymbol{H}}{kT}, \tag{15}$$

that compares the maximum energy per dipole associated to the external field and the thermal energy. Several field strengths have been sampled in the range : $\alpha \in [\,0,\ 45]$. In what follows we will consider uniquely fields oriented perpendicular to the grafting surface of the brush and pointing out of the surface (along the positive z-axis in our system). Finally, another important parameter to characterise the system is the chain grafting density

$$\sigma_g \equiv \frac{N_g}{L^2} \tag{16}$$

where N_g is the number of grafted chains in a square of size L.

In what follows we will focus in the study of how the force created by the monomers of the dipolar brush on the penetrating particle depends on the distance between the grafting surface of the brush and the centre of that particle. In sake of simplicity hereafter we will refer to the set of those forces as the force profile of the brush $F_z(z)$, and the previous distance as the surface-particle distance z.

The results obtained from our simulations for the force profiles of dipolar brushes at zero field can be summarized in Figure 2a,b. These figures correspond to a penetrating particle of diameter $R = 5$ and several grafting densities σ_g. In these figures the brushes are fully dipolar and the chains have twenty monomers each one with their dipole located at the centre of the monomer ($N = N_{dip} = 20$). In sake of comparison we have also added the force profiles for non-dipolar brushes for $\sigma_g = 0.04$. For brushes in good solvent, Figure 2a, the differences between non-dipolar and dipolar brushes for the set of tested parameters show very slight differences except at short surface-particle distances. On the other hand, as Figure 2b shows, non-dipolar brushes in bad solvents exhibit a larger range of action and force profiles with a less abrupt increase in the repulsive force when compared with their dipolar counterpart. It is known from previous works [110], that in dipolar-brushes, specially in the bad-solvent case, the entanglements induced by dipolar interactions inside the brush create a more compact brush structure than in the case of non-dipolar brushes, which explains the observed shorter action range for the dipolar-brushes, and why when the dipolar brush starts to be quite compressed by the penetrating particle, repulsive forces are higher.

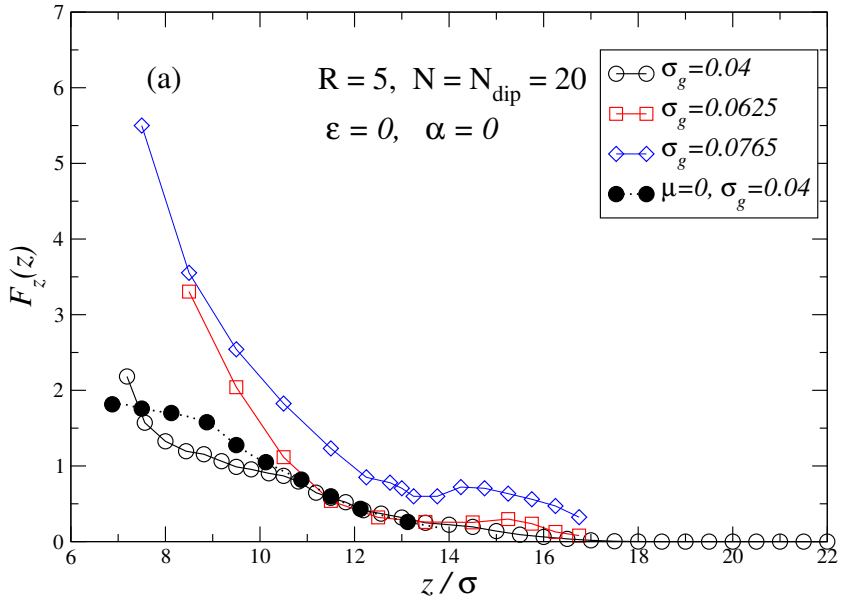

Figure 2. *Cont.*

 doi:10.20944/preprints202412.1431.v1

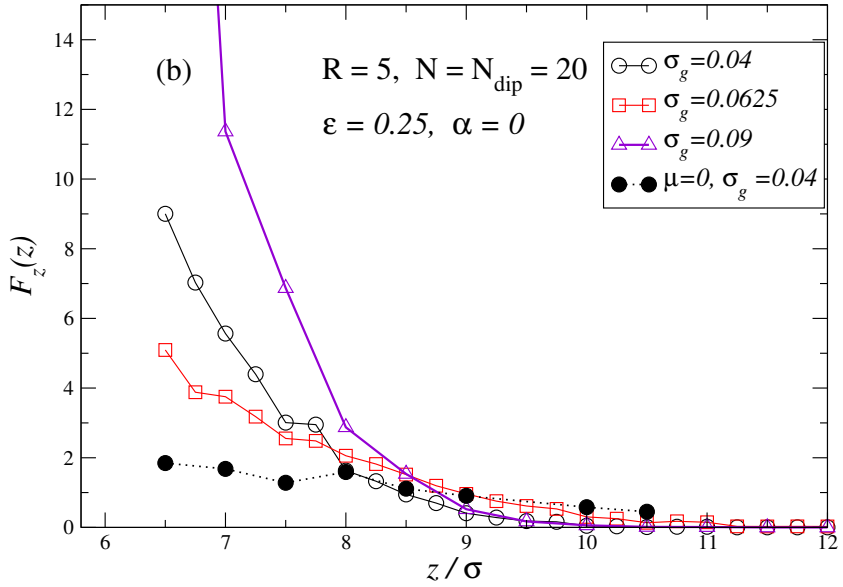

Figure 2. Force profiles along the direction perpendicular to the grafting surface of the dipolar brush as a function of the distance z between the grafting surface and the penetrating particle of radius $R = 5$. The chains of the brushes are fully dipolar $N = N_{dip} = 20$, and no external field is applied $\alpha = 0$. Several brush grafting densities are shown in each plot: $\sigma_g = 0.04, 0.0625, 0.0765, 0.9$. Plot (**a**) depicts the force profiles for brushes in good solvent $\varepsilon = 0$, while plot (**b**) depicts the force profiles for brushes in a bad solvent $\varepsilon = 0.25$ (sticky chains condition). Filled black symbols in each plot represent the force profile obtained for the non-dipolar brush case, $\mu = 0$, at grafting density $\sigma_g = 0.04$.

Previous results at zero field are not very surprising and could be quite easily inferred by relating the monomer density profiles already studied in previous works for dipolar brushes [110] with the steric hindrance they will produce on the penetrating particle. Nonetheless, force profiles suffer a very important transformation when an external field is applied to the dipolar brushes. This can be observed in Figure 3a,b for $\alpha = 9$ and Figure 4a,b for $\alpha = 45$. In those plots all remaining system parameters are kept equal than in Figure 2a,b. Results show the appearance of an initial steep barrier that hampers the penetration of the particle. This barrier is followed by an intermediate region where the repulsive force decreases before increasing again at very short surface-particle distances. In fact, if the grafting density of the brush is large enough, there exists a region in which the brush exerts an attractive force on the penetrating particles (negative values for the force on the force profile). The existence of such attractive forces between the brush and the penetrating particle leads to the existence of a stationary point. The development of a stationary point has important consequences for practical applications as it allows for the intake and retention of colloidal particles or large molecules inside the brush when the field is active, and its ulterior release when the external field is removed.

 doi:10.20944/preprints202412.1431.v1

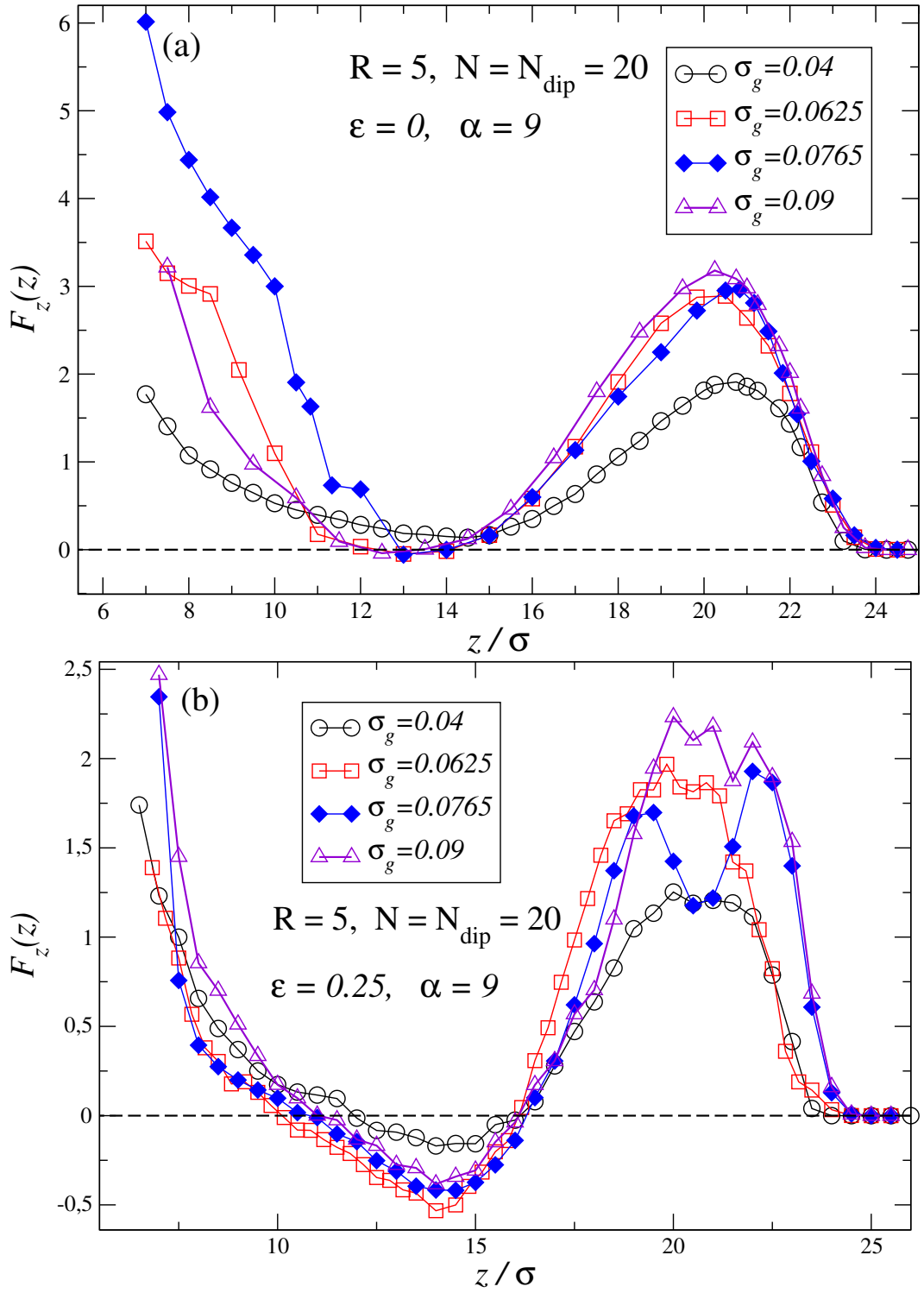

Figure 3. Force profiles for same brushes than in Figure 2 but now under and external moderate field $\alpha = 9$. Plot (**a**) depicts the force profiles for brushes in good solvent $\varepsilon = 0$, while plot (**b**) depicts the force profiles for brushes in a bad solvent $\varepsilon = 0.25$ (sticky chains condition).

 doi:10.20944/preprints202412.1431.v1

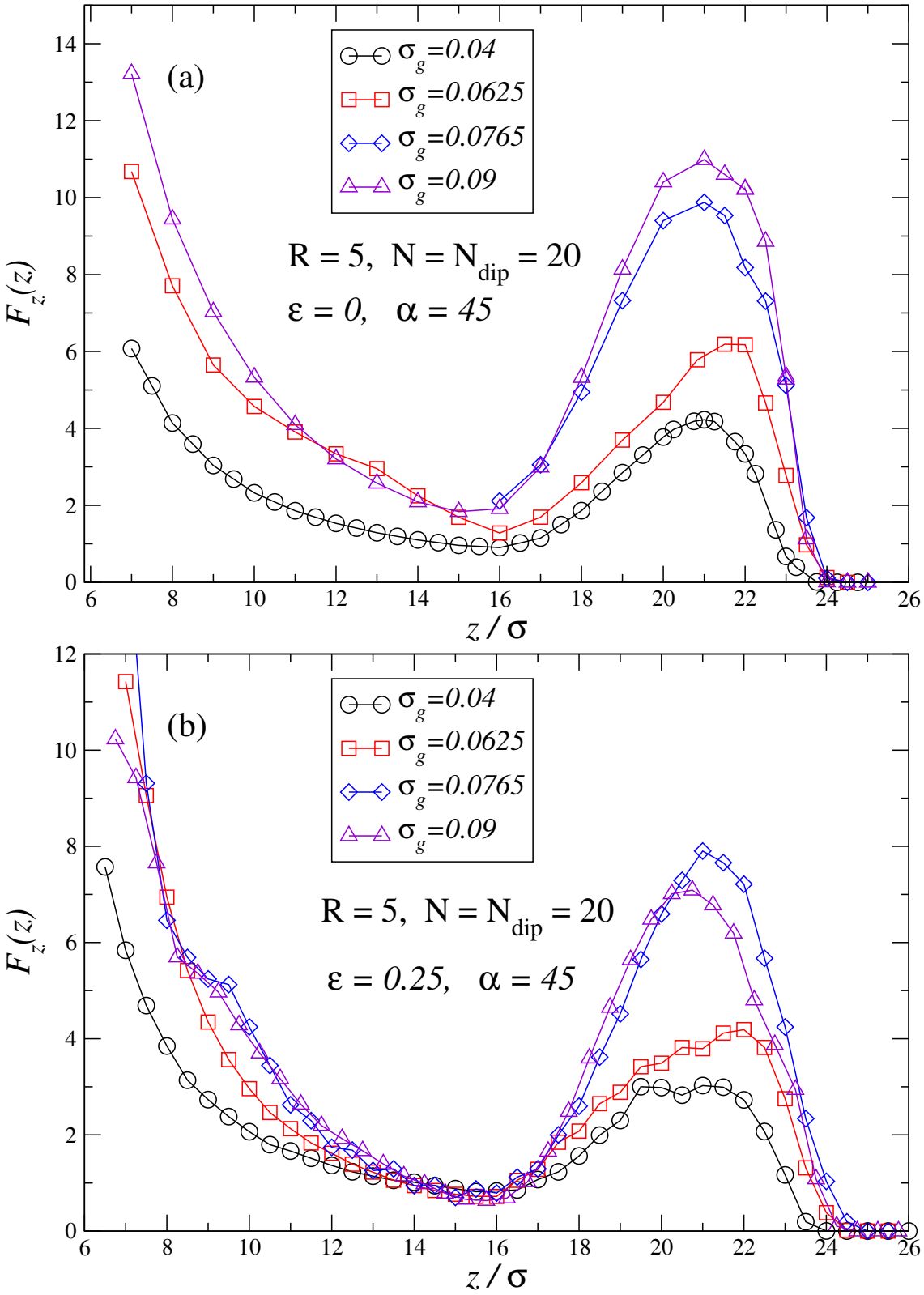

Figure 4. Force profiles for same brushes than in Figures 2 and 3 but now at high field $\alpha = 45$. Plot (**a**) depicts the force profiles for brushes in good solvent $\varepsilon = 0$, while plot (**b**) depicts the force profiles for brushes in a bad solvent $\varepsilon = 0.25$ (sticky chains condition).

 doi:10.20944/preprints202412.1431.v1

A comparison of Figure 3a for good solvent ($\varepsilon = 0$), and Figure 3b for bad solvent ($\varepsilon = 0.25$) shows that in bad solvent, the attractive forces become stronger and the range of surface-particle distances over which the brush exerts an attractive force is much broader. In addition, the comparison reveals that for brushes in bad solvents the initial force barrier at large distances is slightly weaker. In contrast to the zero field case, now profiles for both bad and good solvent exhibit quite similar ranges of action: that can be understood in terms of the fact that now in both solvent conditions, the chains are quite stretched towards the bulk due to the aligning effect of the external field which dominates and leads to very similar chain persistence lengths in both cases.

Figure 3(b) shows that the largest attractive force (the most negative) is obtained for a grafting density of $\sigma_g = 0.0625$: therefore one must conclude that given a field strength and a value for the attractive interaction among monomers, ε, there exists an optimal value of the grafting density that maximizes the attraction that the brush exerts on the penetrating particle. It should be also noticed that for a given dipolar brush, by tuning the strength of the external field one can tune the properties of the force profiles and get the strongest possible attraction between the penetrating particle and the brush.

Figure 4a,b, show the force profiles for similar brush parameters than in previous figures but for $\alpha = 45$. By comparing these new force profiles with the corresponding ones in Figure 3a,b, it is observed that when the strength of the external field is substantially increased, two effects take place: the amplitude of the initial force barrier is increased and, attractive forces cease to exist as the force profile becomes fully repulsive. Nonetheless, even for such high fields still an intermediate region with substantially lower repulsive forces still exists. It should be also observed that the range of action of the force profiles for $\alpha = 45$ remains approximately the same than for $\alpha = 9$ which implies that already for $\alpha = 9$ brush chains are in a quite extended conformation, so a further increase in the external field strength does not substantially modify the extension of the chains although it has deep effects on the force profiles of the brushes.

It remains now to be explained why there is such a dramatic change in the force felt by the penetrating particle when an external field is applied. The initial force barrier felt by the penetrating particle is clearly due to the steric interactions among the monomers of the chains and the penetrating particle: the enhanced persistence length of the dipolar chains onto an applied external field displaces a large amount of monomers far from the grafting surface, and brushes become more resistant to compression. The drop of the repulsive forces once the particle has overcome the initial force barrier can be understood in terms of Kelvin forces: these forces arise from the dipolar mismatch between the non-dipolar parts of our system (the grafting surface and the penetrating particle), and the dipolar media created by the dipolar monomers of the brush chains. A clear example of such Kelvin forces in soft matter occurs for instance in the magnetophoresis of spheres of weak magnetic materials, where the sum of all these forces onto a single particle immersed in a medium can be resumed in the following expression [132]:

$$\boldsymbol{F}_{mag} = \frac{\chi_p - \chi_m}{2\mu_o} V \nabla (\boldsymbol{B})^2, \tag{17}$$

where, χ_p and χ_m represent the volume magnetic susceptibilities of the particle and the medium, respectively. V is the volume of particle, and $\boldsymbol{B} = \mu_0 \boldsymbol{H} + \boldsymbol{M}$, being $\boldsymbol{M}$ the magnetization and μ_o the permeability of the vacuum. Another well known example are inverse ferrofluids [133,134]: these systems can be modelled, in a first approach, as if the magnetic suspension of particles was not present and the non-magnetic particles of radius R were instead bearing an induced magnetic dipole $\boldsymbol{\mu} = -4\pi\beta R^3 \boldsymbol{H}$, where $\beta = (\mu_r - 1)/(2\mu_r + 1)$ characterizes the effective permeability of the magnetic suspension, and μ_r represents the relative permeability of the fluid. This alternative image used to predict the behaviour of inverse ferrofluids will be very useful when discussing our results although unfortunately Equation (17) cannot be applied to provide a quantitative description in our case. This limitation is due on one side to the fact that the particles forming part of the polymeric chains are highly correlated: they are linked forming chains and grafted to a surface, and its density is further perturbed by the non-penetrating particle. Thus, we cannot assume a homogeneous bath of dipolar

 doi:10.20944/preprints202412.1431.v1

particles as the use of Equation (17) implies. Another reason is that the aggregates in suspension have a size that cannot be disregarded respect to the size of the non-dipolar particle (the penetrating particle) which would be another condition to be fulfilled for Equation (17) to hold. On the other hand, the grafting surface is not spherical which also further prevents us from using Equation (17).

It should be noticed that Kelvin forces are only expected to be large in our systems when an external field is applied. The reason for it is that at zero field we can consider those monomers to exhibit a random orientation of their dipoles: there is always a certain correlation among the orientation of the dipoles due to the fact the chains are grafted to the surface, but it has been shown in previous works that it is very small [115]. Therefore the polarization/magnetization of the media is almost zero so Kelvin forces are expected to be almost negligible. On the other hand, when an external field is applied monomers tend to orientate along the external field, so they form a media with a non-zero polarization/magnetization and in these cases Kelvin forces are expected to be of importance to explain the behaviour of the systems.

A quite simple qualitative explanation of the features observed in the force profiles when an external field is applied can be drawn if one proceeds by analogy with inverse ferrofluids and, we consider an alternative but equivalent image of our system: forces observed in our system will be similar to those observed in an hypothetical or alternative system in which the volume occupied by the polymer brush is non-dipolar, but both the grafting surface and the penetrating particle are instead made of dipolar material: inside the dipolar material, in this alternative model, the dipoles point roughly in the opposite direction to that of the external field in our real system, and the modulus of those dipoles increase with the α of our real system. Therefore the surface and penetrating particle have dipoles oriented in a close to nose-tail conformation, and the force between them will be of attractive nature. This attractive force will counteract the repulsive one arising from the steric interactions, and a competition between these two opposite forces will exist.

Therefore, the existence of a net attractive force for the penetrating particle will happen only when attractive Kelvin forces dominate over the repulsive forces created by the steric hindrance among the monomers of the brush and the penetrating particle. It should be noticed than an overcoming by the attractive forces can only happen when the penetrating particle and the surface are not too far as otherwise Kelvin forces will be too weak. In a same way, attractive forces can not overcome repulsive ones when the penetrating particle is too close to the surface, as then the brush is locally so compressed that the steric hindrance is very high. On the other hand, if we increase the grafting density, we then increase the steric hindrance, specially when the particle is close to the grafting surface, so we expect that beyond a certain grafting density threshold the repulsive forces will completely dominate over Kelvin forces. In turn, if we reduce the grafting density we certainly reduce the steric hindrance produced by the monomers, but we also dilute in that case the dipolar media so Kelvin forces also become quite weak in nature. For that reason our simulations point out that there exists an optimal grafting density that shows the largest net attractive force for the penetrating particle, and it also explains why too low or too high grafting densities are not compatible with having a stationary point in the force profile of the penetrating particle.

Another important point to understand is how the dipolar content of the brush at a fixed polymer chain length influences the force profiles felt by the penetrating particle. Figures 5a,b show how the force profiles for brushes with chains of total length $N = 20$ immersed in a bad solvent. The force profiles for brushes made of a different number of dipolar particles in them $N_{dip} = 0,\ 5,\ 10,\ 20$ are shown. In the zero field case, Figure 5a, the most repulsive force profile for intermediate distances between the particle and the grafting surface corresponds to $N_{dip} = 5$. This can be understood as a small amount of sparse dipolar monomers in the chain helps to increase the persistence length of the chain as segments containing dipoles inside a same chain try to align. Nonetheless, when the amount of dipolar monomers is further increased, the interaction among dipoles of neighbouring chains will start to be non-negligible, persistence length will decrease and brushes will start to adopt more collapsed conformations what leads to have a smaller steric hindrance at a same surface-particle distance. For

Preprints.org (www.preprints.org) | NOT PEER-REVIEWED | Posted: 17 December 2024 doi:10.20944/preprints202412.1431.v1

$\alpha = 9$, see Figure 5b, it is observed that the chains tend to be more extended as N_{dip} increases gradually developing the typical force profile observed in previous figures: as already explained in precedent paragraph, a larger dipole content in the brush strengthens the Kelvin forces that can overcome the repulsive steric force leading to the existence of a net attractive force felt by the penetrating particle. Force profiles for $N = N_{dip} \in (5, 40)$ have also been determined (not shown): these force profiles show similar feature to those observed in previous figures but net attractive forces between the penetrating particle and the brush can only be obtained for an intermediate range of polymer lengths: the extension of those ranges depend on the system parameter sets and the strength of the external applied field. This last result can be reasoned as follows: too short chains lead to a dipolar region too small to be able to develop Kelvin forces large enough as to oppose the repulsive steric forces. Moreover, such short chains do not allow for a proper immersion of the penetrating particle inside the dipolar media which also produces small Kelvin forces. On the other hand, when chains are very long, if we resort again to the analogy of an inverse system we did before, we find that once the particle is fully immersed in the brush, the surface-particle distance is still too large for Kelvin forces to be large enough to overcome the steric force. If the particle gets closer to the surface those Kelvin forces will increase, but the monomer density, and thus the steric force will increase. Therefore, when polymer chains are very large, Kelvin forces will never overcome the steric repulsive forces, so the penetrating particle can never feel a net attractive force.

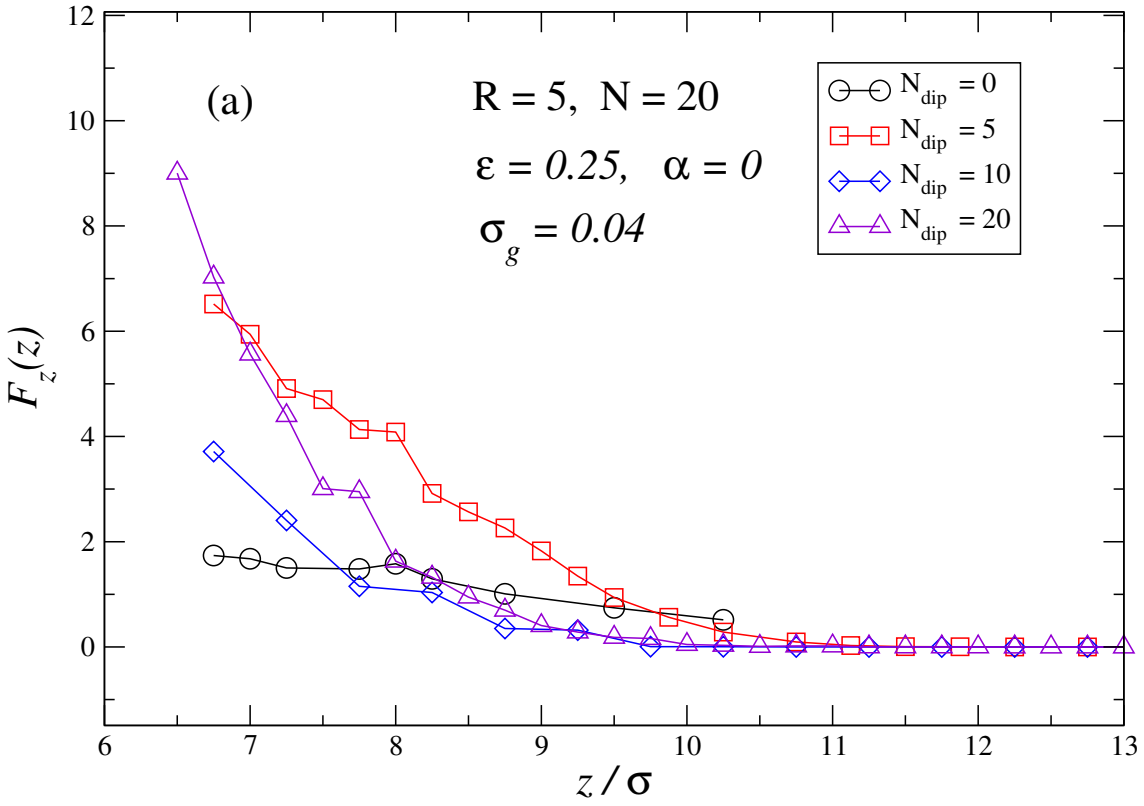

Figure 5. *Cont.*

 doi:10.20944/preprints202412.1431.v1

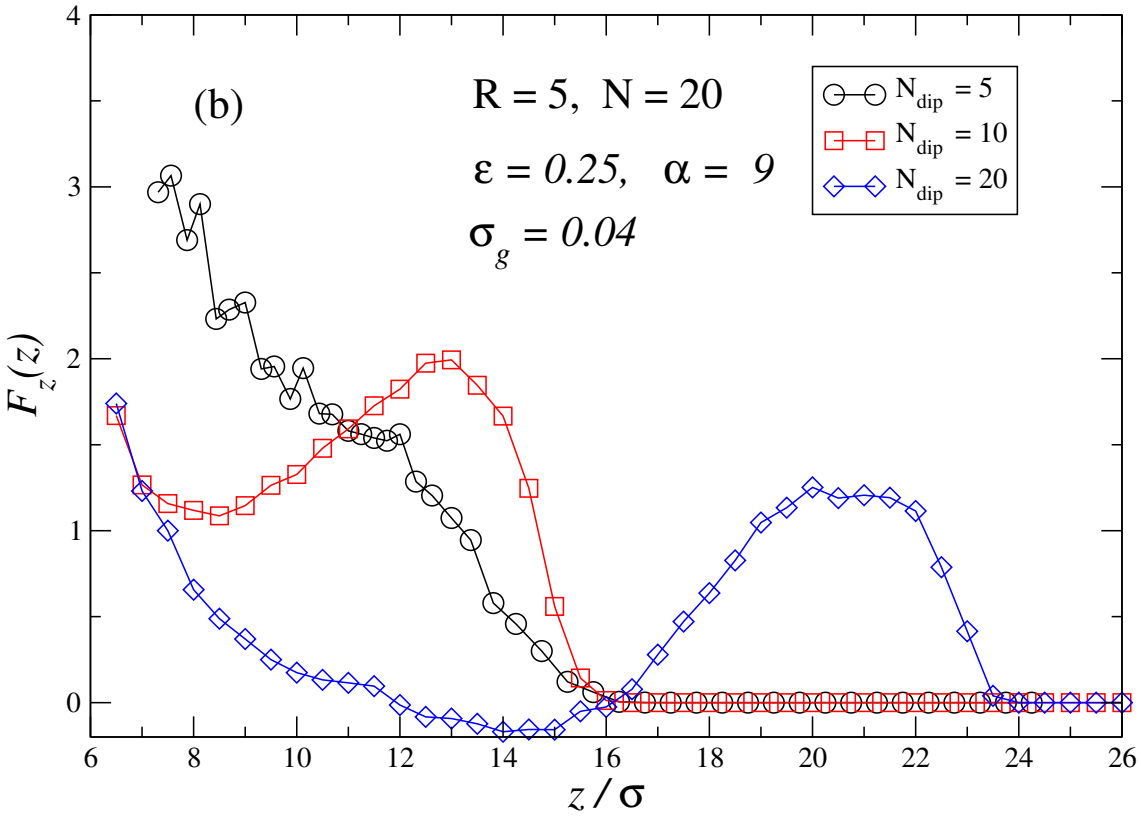

Figure 5. Force profiles representing the force perpendicular to the grafting surface as a function of the distance z between the surface and the centre of the penetrating particle. Brush parameters are similar to previous figures but now the number of dipoles contained in the chain varies as $N_{dip} = 0, 5, 10, 20$, corresponding $N_{dip} = 20$ to a chain where all monomers bear a dipole. The rest of cases, dipoles are equally spaced inside the monomer sequence of the chain. Plot (**a**) corresponds to ($\alpha = 9, \varepsilon = 0$), plot (**b**) corresponds to ($\alpha = 9, \varepsilon = 0.25$).

Finally, it is also very interesting to determine how the force profiles depend on the diameter of the penetrating particle. Figure 6a,c show for several field strengths $\alpha = 0, 9, 45$, respectively, how the force profile varies for diameters $R = 3.5, 5, 7.5$. As expected, we observe that the larger is the diameter of the penetrating particle is, the higher is the initial repulsive force barrier exerted by the brush on the penetrating particle. Nonetheless, as Figure 6b shows, that does not prevent the existence of a region with attractive forces, although the attractive basin is observed to decrease in range with the particle diameter. The rationale behind that behaviour is that although the steric hindrance exerted by the brush increases with the surface of the penetrating particle exposed to the monomers, so does the Kelvin forces which also will increase in strength with the volume of the particle.

 doi:10.20944/preprints202412.1431.v1

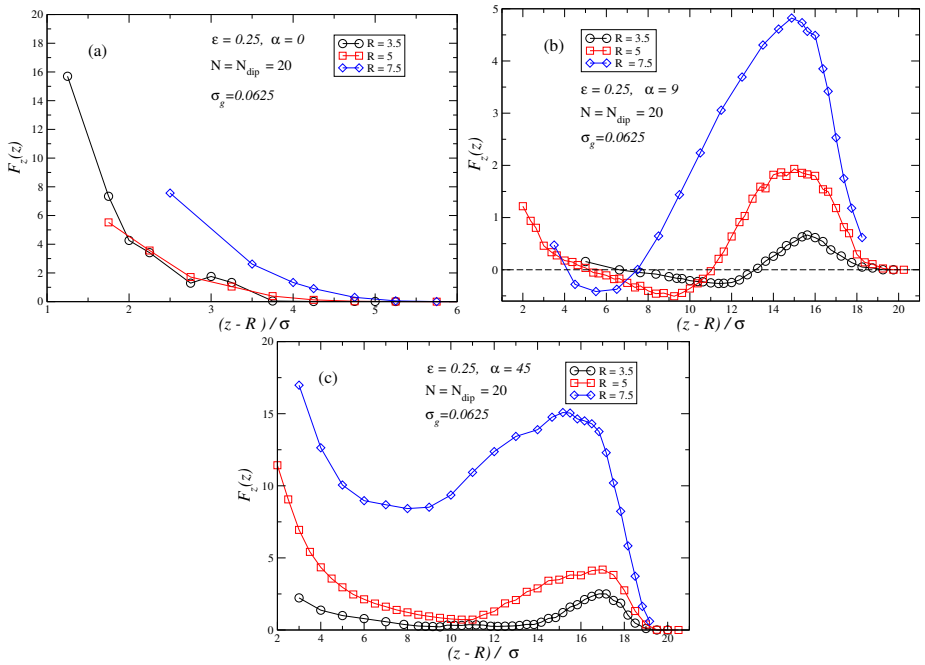

Figure 6. In these plots the dependence of the force profiles as a function of the radius of the penetrating particles is studied for several external fields $\alpha = 0, 9, 45$. Brushes are under bad solvent conditions $\epsilon = 0.25$, the grafting density of the brushes is set to $\sigma_g = 0.0625$ and chains are fully dipolar $N = N_{dip} = 20$.

4. Conclusions

In this work we have studied via numerical simulations the interaction of a penetrating particle with a dipolar colloidal brush. The brush is constructed by grafting many supramolecular polymers onto a common surface, each of which consists of a linked sequence of dipolar and neutral particles (the monomers of the chains). The study has been exemplified using magnetic interactions that constitute a realization of magnetic colloidal brushes, but the conclusions of this work can be easily extended to the case of supramolecular and molecular electric dipolar brushes: the interactions dipole-dipole and dipole-external field are the same, except for a prefactor, for magnetic and electric dipoles.

Force profiles for penetrating particles of different sizes have been determined for a wide set of grafting densities, solvent conditions, chain lengths and dipolar content of the brushes. In the absence of an external field dipolar brushes are observed to exhibit rather monotonous force profiles that are a reflection of the steric hindrance created by the compactness of the brushes. As expected bad solvents tend to promote more compactified brush structures which in turn produce force profiles of shorter range but with a steep increase in the force as surface-particle distance reduces. An important modification in the force profiles occurs when an external field is applied perpendicular to the grafting surface. In that case, in addition to the expected extension of the chains [115] that translates into an extended action range of the force profiles, a force barrier at large distances from the surface develops. These barriers increase in height with the field, and also with the grafting density: nonetheless, there exists a grafting density threshold beyond which the barrier does not growth further in heigh rather it decreases slightly. Another important feature of the force profiles under an external field is that there is an intermediate range of surface-particle distances in which repulsion forces are drastically reduced. For bad solvent and moderated field strengths, the forces in this intermediate regime of distances can turn even from repulsive to attractive and lead to the existence of an stationary point in which penetrating particles will tend to remain entrapped inside the brush. This quite unexpected attraction between the brush and the penetrating particle can be reasoned, as explained in further detail in previous section, as the result of an equilibrium between two opposite forces: the entropic or

 doi:10.20944/preprints202412.1431.v1

steric repulsive force due to the high density of monomers near the grafting surface, and an attractive force emerging from Kelvin forces due to the mismatch between the dipolar media created by the dipolar monomers of the brush, and the non-dipolar media existing inside the particle and the grafting surface. As the strength of both forces depends on the external field applied, it is possible by tuning the external field to induce larger or smaller attractive forces onto the penetrating particle. Through this competition between steric repulsive forces and Kelvin forces it is also possible to explain qualitatively some other observed results: given a grafting density of chains, there exists an optimal value of the external field that maximizes the attraction between the brush and the penetrating particle; brushes with polymer chains too short or too long will not lead to regions inside the brush where the brush attracts the penetrating particle; for penetrating particles of larger size the force barrier becomes increasingly more repulsive, but that fact does not preclude the existence of stable points for the penetrating particle inside the brush.

The possibility to induce via external fields force profiles with stationary points can be used to favour applications of polymer brushes in which the entrapping and retention of colloidal particles for a later release is required. On the other hand the possibility to create and control the strength of force barriers at a certain distance of the grafting surface can also be used, among other applications, to control the rate of adsorption and reactivity of catalytic surfaces. The results obtained in this work also envisage the potential of dipolar brushes in the field of self-assembly, the fabrication of materials based on self-organized colloidal structures, protein crystallization assistance, shape and size selection of colloidal particles, among other uses.

This study constitutes a first step towards the understanding of dipolar colloidal brushes interaction with colloidal particles in solution. Next steps in the understanding of these systems comprises the study of the force profiles for non-spherical colloids and molecules, as well as the development of analytic frameworks to accurately predict the forces involved and the resulting force profile. We expect our work will stimulate further developments on this subject of increasing scientific interest.

Author Contributions: Conceptualization, J.C.; methodology, J.C. .; software, J.C., A.F.; validation, A.C. and J.B.; formal analysis, J.C., A.F. ; investigation, J.C., A.F., A.C., J.B; resources, J.C ; data curation, J.C. ; writing—original draft preparation, A.F. and J.C.; writing—review and editing, A.C, J.B. ; visualization, J.C.; supervision, J.C.; project administration, J.C. All authors have read and agreed to the published version of the manuscript.

Funding: All authors thank the financial support of the Spanish Ministry of Economy and Competitiveness (MINECO/AEI/FEDER,UE) through the projects *Proyecto de I+D (excelencia) DPI2017-86610-P* and *PID2020-118317GB-I00 / AEI /10.13039/501100011033*.

Institutional Review Board Statement: Not applicable.

Informed Consent Statement: Not applicable.

Data Availability Statement: Dataset available on request from the authors.

Acknowledgments: All authors thank Pedro Sánchez from the University of Wien for his careful reading of the manuscript.

Conflicts of Interest: The authors declare no conflicts of interest.

References

1. Zhang, Y.; Li, M.; Li, B.; Sheng, W. Surface Functionalization with Polymer Brushes via Surface-Initiated Atom Transfer Radical Polymerization: Synthesis, Applications, and Current Challenges. *LANGMUIR* **2024**, *40*, 5571–5589. doi:10.1021/acs.langmuir.3c03647.
2. Wang, C.; Zhao, H. Polymer Brushes and Surface Nanostructures: Molecular Design, Precise Synthesis, and Self-Assembly. *LANGMUIR* **2024**, *40*, 2439–2464. doi:10.1021/acs.langmuir.3c02813.
3. Feng, Y.; Wei, C.; Zhao, T. Molecular brushes based on poly(amino acid)s: synthesis, structures, and applications. *JOURNAL OF POLYMER SCIENCE* **2024**, *62*, 480–491. doi:10.1002/pol.20230461.
4. Wang, R.; Wei, Q.; Sheng, W.; Yu, B.; Zhou, F.; Li, B. Driving Polymer Brushes from Synthesis to Functioning. *ANGEWANDTE CHEMIE-INTERNATIONAL EDITION* **2023**. doi:10.1002/anie.202219312.

5. Metze, F.K.; Klok, H.A. Supramolecular Polymer Brushes. *ACS POLYMERS AU* **2023**, *3*, 228–238. doi:10.1021/acspolymersau.2c00067.
6. Peng, H.Q.; Zhu, W.; Guo, W.J.; Li, Q.; Ma, S.; Bucher, C.; Liu, B.; Ji, X.; Huang, F.; Sessler, J.L. Supramolecular polymers: Recent advances based on the types of underlying interactions. *PROGRESS IN POLYMER SCIENCE* **2023**, *137*. doi:10.1016/j.progpolymsci.2022.101635.
7. Wang, C.; Zhao, H. Polymer brush-based nanostructures: from surface self-assembly to surface co-assembly. *SOFT MATTER* **2022**, *18*, 5138–5152. doi:10.1039/d2sm00458e.
8. Yin, L.; Liu, L.; Zhang, N. Brush-like polymers: design, synthesis and applications. *CHEMICAL COMMUNICATIONS* **2021**, *57*, 10484–10499. doi:10.1039/d1cc03940g.
9. Yang, R.; Wang, X.; Yan, S.; Dong, A.; Luan, S.; Yin, J. Advances in design and biomedical application of hierarchical polymer brushes. *PROGRESS IN POLYMER SCIENCE* **2021**, *118*. doi:10.1016/j.progpolymsci.2021.101409.
10. Reese, C.J.; Boyes, S.G. New methods in polymer brush synthesis: Non-vinyl-based semiflexible and rigid-rod polymer brushes. *PROGRESS IN POLYMER SCIENCE* **2021**, *114*. doi:10.1016/j.progpolymsci.2021.101361.
11. Ma, S.; Zhang, X.; Yu, B.; Zhou, F. Brushing up functional materials. *NPG ASIA MATERIALS* **2019**, *11*. doi:10.1038/s41427-019-0121-2.
12. Conrad, J.C.; Robertson, M.L. Towards mimicking biological function with responsive surface-grafted polymer brushes. *Current Opinion in Solid State and Materials Science* **2019**, *23*, 1–12. Active and adaptive soft matter, doi:https://doi.org/10.1016/j.cossms.2018.09.004.
13. Xu, X.; Billing, M.; Ruths, M.; Klok, H.A.; Yu, J. Structure and Functionality of Polyelectrolyte Brushes: A Surface Force Perspective. *Chemistry – An Asian Journal* **2018**, *13*, 3411–3436, [https://aces.onlinelibrary.wiley.com/doi/pdf/10.1002/asia.201800920]. doi:https://doi.org/10.1002/asia.201800920.
14. Welch, M.E.; Ober, C.K. Responsive and patterned polymer brushes. *JOURNAL OF POLYMER SCIENCE PART B-POLYMER PHYSICS* **2013**, *51*, 1457–1472. doi:10.1002/polb.23356.
15. Lokesh, M.G.; Tiwari, A.K. A concise review on polymer brushes and its interaction with surfactants: An approach towards smart materials. *JOURNAL OF MOLECULAR LIQUIDS* **2024**, *407*. doi:10.1016/j.molliq.2024.125168.
16. Conrad, J.C.; Robertson, M.L. Shaping the Structure and Response of Surface-Grafted Polymer Brushes via the Molecular Weight Distribution. *JACS AU* **2023**. doi:10.1021/jacsau.2c00638.
17. Liu, Y.; Wu, Y.; Zhou, F. Shear-Stable Polymer Brush Surfaces. *LANGMUIR* **2023**, *39*, 37–44. doi:10.1021/acs.langmuir.2c03012.
18. Zimmermann, R.; Duval, J.F.L.; Werner, C.; Sterling, J.D. Quantitative insights into electrostatics and structure of polymer brushes from microslit electrokinetic experiments and advanced modelling of interfacial electrohydrodynamics. *CURRENT OPINION IN COLLOID & INTERFACE SCIENCE* **2022**, *59*. doi:10.1016/j.cocis.2022.101590.
19. Geoghegan, M. Weak polyelectrolyte brushes. *SOFT MATTER* **2022**, *18*, 2500–2511. doi:10.1039/d2sm00005a.
20. Xu, X.; Billing, M.; Ruths, M.; Klok, H.A.; Yu, J. Structure and Functionality of Polyelectrolyte Brushes: A Surface Force Perspective. *CHEMISTRY-AN ASIAN JOURNAL* **2018**, *13*, 3411–3436. doi:10.1002/asia.201800920.
21. Wang, S.; Jing, B.; Zhu, Y. Molecule Motion at Polymer Brush Interfaces from Single-Molecule Experimental Perspectives. *JOURNAL OF POLYMER SCIENCE PART B-POLYMER PHYSICS* **2014**, *52*, 85–103. doi:10.1002/polb.23414.
22. Reznik, C.; Landes, C.F. Transport in Supported Polyelectrolyte Brushes. *ACCOUNTS OF CHEMICAL RESEARCH* **2012**, *45*, 1927–1935. doi:10.1021/ar3001537.
23. Ballauff, M. Spherical polyelectrolyte brushes. *PROGRESS IN POLYMER SCIENCE* **2007**, *32*, 1135–1151. doi:10.1016/j.progpolymsci.2007.05.002.
24. Ballauff, M.; Borisov, O. Polyelectrolyte brushes. *CURRENT OPINION IN COLLOID & INTERFACE SCIENCE* **2006**, *11*, 316–323. doi:10.1016/j.cocis.2006.12.002.
25. Das, S.; Banik, M.; Chen, G.; Sinha, S.; Mukherjee, R. Polyelectrolyte brushes: theory, modelling, synthesis and applications. *SOFT MATTER* **2015**, *11*, 8550–8583. doi:10.1039/c5sm01962a.

26. Mikhailov, V, I.; Darinskii, A.A.; Birshtein, T.M. Bending Rigidity of Branched Polymer Brushes with Finite Membrane Thickness. *POLYMER SCIENCE SERIES C* **2022**, *64*, 110–122. doi:10.1134/S1811238222700199.
27. Niu, Y.; Bu, X.; Zhang, X. Single Chain Mean-Field Theory Study on Responsive Behavior of Semiflexible Polymer Brush. *MATERIALS* **2021**, *14*. doi:10.3390/ma14040778.
28. Klushin, L.I.; Skvortsov, A.M.; Qi, S.; Schmid, F. Polydisperse Brush with the Linear Density Profile. *POLYMER SCIENCE SERIES C* **2018**, *60*, 84–94.
29. Zhulina, E.B.; Borisov, O.V. Dendritic polyelectrolyte brushes. *POLYMER SCIENCE SERIES C* **2017**, *59*, 106–118. doi:10.1134/S1811238217010143.
30. Wang, Z.; Li, B.H. Self-assembly of block copolymers grafted onto a flat substrate: Recent progress in theory and simulations. *CHINESE PHYSICS B* **2016**, *25*. doi:10.1088/1674-1056/25/1/016402.
31. Binder, K.; Milchev, A. Polymer brushes on flat and curved surfaces: How computer simulations can help to test theories and to interpret experiments. *JOURNAL OF POLYMER SCIENCE PART B-POLYMER PHYSICS* **2012**, *50*, 1515–1555. doi:10.1002/polb.23168.
32. Tagliazucchi, M.; Szleifer, I. Stimuli-responsive polymers grafted to nanopores and other nano-curved surfaces: structure, chemical equilibrium and transport. *SOFT MATTER* **2012**, *8*, 7292–7305. doi:10.1039/c2sm25777g.
33. Xu, X.; Cao, D.; Wu, J. Density functional theory for predicting polymeric forces against surface fouling. *SOFT MATTER* **2010**, *6*, 4631–4646. doi:10.1039/c0sm00034e.
34. Naji, A.; Seidel, C.; Netz, R.R. Theoretical approaches to neutral and charged polymer brushes. In *SURFACE- INITIATED POLYMERIZATION II*; Jordan, R., Ed.; SPRINGER-VERLAG BERLIN: HEIDELBERGER PLATZ 3, D-14197 BERLIN, GERMANY, 2006; Vol. 198, *Advances in Polymer Science*, pp. 149–183. doi:10.1007/12_062.
35. Rühe, J.; Ballauff, M.; Biesalski, M.; Dziezok, P.; Gröhn, F.; Johannsmann, D.; Houbenov, N.; Hugenberg, N.; Konradi, R.; Minko, S.; Motornov, M.; Netz, R.; Schmidt, M.; Seidel, C.; Stamm, M.; Stephan, T.; Usov, D.; Zhang, H. Polyelectrolyte brushes. In *POLYELECTROLYTES WITH DEFINED MOLECULAR ARCHITECTURE I*; Schmidt, M., Ed.; SPRINGER-VERLAG BERLIN: HEIDELBERGER PLATZ 3, D-14197 BERLIN, GERMANY, 2004; Vol. 165, *Advances in Polymer Science*, pp. 79–150. doi:10.1007/b11268.
36. Vorsmann, C.F.; Del Galdo, S.; Capone, B.; Locatelli, E. Colloidal adsorption in planar polymeric brushes. *Nanoscale Adv.* **2024**, *6*, 816–825. doi:10.1039/D3NA00598D.
37. Dimitrov, D.; Milchev, A.; Binder, K. Polymer brushes on flat and curved substrates: Scaling concepts and computer simulations. Macromolecular symposia. Wiley Online Library, 2007, Vol. 252, pp. 47–57.
38. Kreer, T. Polymer-brush lubrication: a review of recent theoretical advances. *SOFT MATTER* **2016**, *12*, 3479–3501. doi:10.1039/c5sm02919h.
39. Larin, D.E.; Govorun, E.N. Surfactant-Induced Patterns in Polymer Brushes. *Langmuir* **2017**, *33*, 8545–8552. PMID: 28759241, doi:10.1021/acs.langmuir.7b01850.
40. Ishraaq, R.; Das, S. All-atom molecular dynamics simulations of polymer and polyelectrolyte brushes. *CHEMICAL COMMUNICATIONS* **2024**, *60*, 6093–6129. doi:10.1039/d4cc01557f.
41. Abdelbar, M.A.A.; Ewen, J.P.P.; Dini, D.; Angioletti-Uberti, S. Polymer brushes for friction control: Contributions of molecular simulations. *BIOINTERPHASES* **2023**, *18*. doi:10.1116/6.0002310.
42. Binder, K.; Kreer, T.; Milchev, A. Polymer brushes under flow and in other out-of-equilibrium conditions. *SOFT MATTER* **2011**, *7*, 7159–7172. doi:10.1039/c1sm05212h.
43. Descas, R.; Sommer, J.U.; Blumen, A. Grafted Polymer Chains Interacting with Substrates: Computer Simulations and scaling. *MACROMOLECULAR THEORY AND SIMULATIONS* **2008**, *17*, 429–453. doi:10.1002/mats.200800046.
44. Viduna, D.; Limpouchová, Z.; Procházka, K. Monte Carlo simulation of polymer brushes in narrow pores. *JOURNAL OF CHEMICAL PHYSICS* **2001**, *115*, 7309–7318. doi:10.1063/1.1405444.
45. Grest, G. Normal and shear forces between polymer brushes. In *POLYMERS IN CONFINED ENVIRONMENTS*; Granick, S., Ed.; SPRINGER-VERLAG BERLIN: HEIDELBERGER PLATZ 3, D-14197 BERLIN, GERMANY, 1999; Vol. 138, *Advances in Polymer Science*, pp. 149–183.
46. Grest, G. Computer simulations of shear and friction between polymer brushes. *CURRENT OPINION IN COLLOID & INTERFACE SCIENCE* **1997**, *2*, 271–277. doi:10.1016/S1359-0294(97)80035-0.
47. Mikhailov, I.V.; Amoskov, V.M.; Darinskii, A.A.; Birshtein, T.M. The Structure of Dipolar Polymer Brushes and Their Interaction in the Melt. Impact of Chain Stiffness. *Polymers* **2020**, *12*. doi:10.3390/polym12122887.

48. Birshtein, T.; Polotsky, A.; Glova, A.; Amoskov, V.; Mercurieva, A.; Nazarychev, V.; Lyulin, S. How to fold back grafted chains in dipolar brushes. *Polymer* **2018**, *147*, 213–224. doi:https://doi.org/10.1016/j.polymer.2018.05.076.
49. Okrugin, B.M.; Richter, R.P.; Leermakers, F.A.M.; Neelov, I.M.; Zhulina, E.B.; Borisov, O.V. Electroresponsive Polyelectrolyte Brushes Studied by Self-Consistent Field Theory. *Polymers* **2020**, *12*. doi:10.3390/polym12040898.
50. Lukiev, I.V.; Mogelnitskaya, Y.A.; Mikhailov, I.V.; Darinskii, A.A. Chains Stiffness Effect on the Vertical Segregation of Mixed Polymer Brushes in Selective Solvent. *Polymers* **2023**, *15*. doi:10.3390/polym15030644.
51. Kielbasa, A.; Kowalczyk, K.; Chajec-Gierczak, K.; Bala, J.; Zapotoczny, S. Applications of surface-grafted polymer brushes with various architectures. *POLYMERS FOR ADVANCED TECHNOLOGIES* **2024**, *35*. doi:10.1002/pat.6397.
52. Chen, W.L.; Cordero, R.; Tran, H.; Ober, C.K. 50th Anniversary Perspective: Polymer Brushes: Novel Surfaces for Future Materials. *Macromolecules* **2017**, *50*, 4089–4113. doi:10.1021/acs.macromol.7b00450.
53. Su, N. Advances and Prospects in the Study of Spherical Polyelectrolyte Brushes as a Dopant for Conducting Polymers. *MOLECULES* **2024**, *29*. doi:10.3390/molecules29061315.
54. Hartmann, S.; Diekmann, J.; Greve, D.; Thiele, U. Drops on Polymer Brushes: Advances in Thin-Film Modeling of Adaptive Substrates. *LANGMUIR* **2024**, *40*, 4001–4021. doi:10.1021/acs.langmuir.3c03313.
55. Atif, M.; Balasini, A. Mixed polymer brushes for controlled protein adsorption: state of the art and future prospective. *MATERIALS ADVANCES* **2024**, *5*, 1420–1439. doi:10.1039/d3ma00935a.
56. Liu, J.; Tang, K.; Wang, M.; Shen, C.; Deng, R. Recent Progress in Janus Nano-Objects with Asymmetric Polymer Brushes. *CHEMISTRY-AN ASIAN JOURNAL* **2024**, *19*. doi:10.1002/asia.202301023.
57. Bhayo, A.M.; Yang, Y.; He, X. Polymer brushes: Synthesis, characterization, properties and applications. *PROGRESS IN MATERIALS SCIENCE* **2022**, *130*. doi:10.1016/j.pmatsci.2022.101000.
58. Poisson, J.; Hudson, Z.M. Luminescent Surface-Tethered Polymer Brush Materials. *CHEMISTRY-A EUROPEAN JOURNAL* **2022**, *28*. doi:10.1002/chem.202200552.
59. Pradhan, S.S.; Saha, S. Advances in design and applications of polymer brush modified anisotropic particles. *ADVANCES IN COLLOID AND INTERFACE SCIENCE* **2022**, *300*. doi:10.1016/j.cis.2021.102580.
60. van Eck, G.C.R.; Chiappisi, L.; de Beer, S. Fundamentals and Applications of Polymer Brushes in Air. *ACS APPLIED POLYMER MATERIALS* **2022**. doi:10.1021/acsapm.1c01615.
61. Zhang, B.y.; Luo, H.n.; Zhang, W.; Liu, Y. Research progress in self-oscillating polymer brushes. *RSC ADVANCES* **2022**, *12*, 1366–1374. doi:10.1039/d1ra07374e.
62. Nakamura, S.; Mitomo, H.; Ijiro, K. Assembly and Active Control of Nanoparticles using Polymer Brushes as a Scaffold. *CHEMISTRY LETTERS* **2021**, *50*, 361–370. doi:10.1246/cl.200767.
63. Li, D.; Xu, L.; Wang, J.; Gautrot, J.E. Responsive Polymer Brush Design and Emerging Applications for Nanotheranostics. *ADVANCED HEALTHCARE MATERIALS* **2021**, *10*. doi:10.1002/adhm.202000953.
64. Li, M.; Pester, C.W. Mixed Polymer Brushes for "Smart" Surfaces. *POLYMERS* **2020**, *12*. doi:10.3390/polym12071553.
65. Wang, S.; Wang, Z.; Li, J.; Li, L.; Hu, W. Surface-grafting polymers: from chemistry to organic electronics. *MATERIALS CHEMISTRY FRONTIERS* **2020**, *4*, 692–714. doi:10.1039/c9qm00450e.
66. Heggestad, J.T.; Fontes, C.M.; Joh, D.Y.; Hucknall, A.M.; Chilkoti, A. In Pursuit of Zero 2.0: Recent Developments in Nonfouling Polymer Brushes for Immunoassays. *ADVANCED MATERIALS* **2020**, *32*. doi:10.1002/adma.201903285.
67. Xiao, S.; Ren, B.; Huang, L.; Shen, M.; Zhang, Y.; Zhong, M.; Yang, J.; Zheng, J. Salt-responsive zwitterionic polymer brushes with anti-polyelectrolyte property. *CURRENT OPINION IN CHEMICAL ENGINEERING* **2018**, *19*, 86–93. doi:10.1016/j.coche.2017.12.008.
68. Keating, J.J.; Imbrogno, J.; Belfort, G. Polymer Brushes for Membrane Separations: A Review. *ACS APPLIED MATERIALS & INTERFACES* **2016**, *8*, 28383–28399. doi:10.1021/acsami.6b09068.
69. Yu, Q.; Ista, L.K.; Gu, R.; Zauscher, S.; Lopez, G.P. Nanopatterned polymer brushes: conformation, fabrication and applications. *NANOSCALE* **2016**, *8*, 680–700. doi:10.1039/c5nr07107k.
70. Azzaroni, O. Polymer brushes here, there, and everywhere: Recent advances in their practical applications and emerging opportunities in multiple research fields. *JOURNAL OF POLYMER SCIENCE PART A-POLYMER CHEMISTRY* **2012**, *50*, 3225–3258. doi:10.1002/pola.26119.

71. Mocny, P.; Klok, H.A. Tribology of surface-grafted polymer brushes. *MOLECULAR SYSTEMS DESIGN & ENGINEERING* **2016**, *1*, 141–154. doi:10.1039/c5me00010f.
72. Kim, J.U.; Matsen, M.W. Repulsion Exerted on a Spherical Particle by a Polymer Brush. *Macromolecules* **2008**, *41*, 246–252. doi:10.1021/ma071906t.
73. Egorov, S.A. Insertion of nanoparticles into polymer brush under variable solvent conditions. *The Journal of Chemical Physics* **2012**, *137*, 134905, [https://pubs.aip.org/aip/jcp/article-pdf/doi/10.1063/1.4757017/15454558/134905_1_online.pdf]. doi:10.1063/1.4757017.
74. Lian, Z.; Qi, S.; Zhou, J.; Schmid, F. Solvent Determines Nature of Effective Interactions between Nanoparticles in Polymer Brushes. *The Journal of Physical Chemistry B* **2015**, *119*, 4099–4108. PMID: 25706324, doi:10.1021/jp511911g.
75. Santo, K.P.; Vishnyakov, A.; Brun, Y.; Neimark, A.V. Adhesion and Separation of Nanoparticles on Polymer-Grafted Porous Substrates. *Langmuir* **2018**, *34*, 1481–1496. PMID: 28914540, doi:10.1021/acs.langmuir.7b02914.
76. Xu, X.; Cao, D.; Wu, J. Density functional theory for predicting polymeric forces against surface fouling. *Soft Matter* **2010**, *6*, 4631–4646. doi:10.1039/C0SM00034E.
77. Milchev, A.; Dimitrov, D.; Binder, K. Excess free energy of nanoparticles in a polymer brush. *Polymer* **2008**, *49*, 3611–3618. doi:https://doi.org/10.1016/j.polymer.2008.04.032.
78. Ermilov, V.; Lazutin, A.; Halperin, A. Colloids in Brushes: The Insertion Free Energy via Monte Carlo Simulation with Umbrella Sampling. *Macromolecules* **2010**, *43*, 3511–3520. doi:10.1021/ma9027273.
79. Milchev, A.; Dimitrov, D.I.; Binder, K. Polymer brushes with nanoinclusions under shear: A molecular dynamics investigation. *Biomicrofluidics* **2010**, *4*, 032202, [https://pubs.aip.org/aip/bmf/article-pdf/doi/10.1063/1.3396446/14587334/032202_1_online.pdf]. doi:10.1063/1.3396446.
80. Merlitz, H.; Wu, C.X.; Sommer, J.U. Inclusion Free Energy of Nanoparticles in Polymer Brushes. *Macromolecules* **2012**, *45*, 8494–8501. doi:10.1021/ma301781b.
81. Zhang, Q.; Xiang, X. Adsorption of a spherical nanoparticle in polymer brushes: Brownian dynamics investigation. *Physica A: Statistical Mechanics and its Applications* **2013**, *392*, 3857–3862. doi:https://doi.org/10.1016/j.physa.2013.05.001.
82. de Beer, S.; Mensink, L.I.S.; Kieviet, B.D. Geometry-Dependent Insertion Forces on Particles in Swollen Polymer Brushes. *Macromolecules* **2016**, *49*, 1070–1078. doi:10.1021/acs.macromol.5b01960.
83. Gao, H.M.; Li, B.; Zhang, R.; Sun, Z.Y.; Lu, Z.Y. Free energy for inclusion of nanoparticles in solvated polymer brushes from molecular dynamics simulations. *The Journal of Chemical Physics* **2020**, *152*, 094905, [https://pubs.aip.org/aip/jcp/article-pdf/doi/10.1063/5.0002257/15575067/094905_1_online.pdf]. doi:10.1063/5.0002257.
84. Spencer, R.K.W.; Ha, B.Y. How a Polymer Brush Interacts with Inclusions and Alters Their Interaction. *Macromolecules* **2021**, *54*, 1304–1313, [https://doi.org/10.1021/acs.macromol.0c02179]. doi:10.1021/acs.macromol.0c02179.
85. Laktionov, M.Y.; Shavykin, O.V.; Leermakers, F.A.M.; Zhulina, E.B.; Borisov, O.V. Colloidal particles interacting with a polymer brush: a self-consistent field theory. *Phys. Chem. Chem. Phys.* **2022**, *24*, 8463–8476. doi:10.1039/D1CP04834A.
86. Offner, A.; Ramon, G.Z. The interaction of a particle and a polymer brush coating a permeable surface. *Journal of Fluid Mechanics* **2021**, *913*, R3. doi:10.1017/jfm.2021.23.
87. Laktionov, M.Y.; Zhulina, E.B.; Klushin, L.; Richter, R.P.; Borisov, O.V. Selective Colloid Transport across Planar Polymer Brushes. *Macromolecular Rapid Communications* **2023**, *44*, 2200980, [https://onlinelibrary.wiley.com/doi/pdf/10.1002/marc.202200980]. doi:https://doi.org/10.1002/marc.202200980.
88. Tom, A.M.; Kim, W.K.; Hyeon, C. Polymer brush-induced depletion interactions and clustering of membrane proteins. *The Journal of Chemical Physics* **2021**, *154*, 214901, [https://pubs.aip.org/aip/jcp/article-pdf/doi/10.1063/5.0048554/15618870/214901_1_online.pdf]. doi:10.1063/5.0048554.

89. Nourbakhsh, S.; Yu, L.; Ha, B.Y. Modeling the Protective Role of Bacterial Lipopolysaccharides against Membrane-Rupturing Peptides. *The Journal of Physical Chemistry B* **2021**, *125*, 8839–8854, [https://doi.org/10.1021/acs.jpcb.1c02330]. PMID: 34319722, doi:10.1021/acs.jpcb.1c02330.
90. Astier, S.; Johnson, E.C.; Norvilaite, O.; Varlas, S.; Brotherton, E.E.; Sanderson, G.; Leggett, G.J.; Armes, S.P. Controlling Adsorption of Diblock Copolymer Nanoparticles onto an Aldehyde-Functionalized Hydrophilic Polymer Brush via pH Modulation. *Langmuir* **2024**, *40*, 3667–3676, [https://doi.org/10.1021/acs.langmuir.3c03392]. PMID: 38320303, doi:10.1021/acs.langmuir.3c03392.
91. Popova, T.O.; Borisov, O.V.; Zhulina, E.B. Polyelectrolyte Brushes with Protein-Like Nanocolloids. *Langmuir* **2024**, *40*, 1232–1246, [https://doi.org/10.1021/acs.langmuir.3c02556]. PMID: 38176061, doi:10.1021/acs.langmuir.3c02556.
92. Gorka, W.; Kuciel, T.; Nalepa, P.; Lachowicz, D.; Zapotoczny, S.; Szuwarzynski, M. Homogeneous Embedding of Magnetic Nanoparticles into Polymer Brushes during Simultaneous Surface-Initiated Polymerization. *Nanomaterials* **2019**, *9*, 456. doi:https://doi.org/10.3390/nano9030456.
93. San Choi, W.; Young Koo, H.; Young Kim, J.; .; Huck, W.T.S. Collective Behavior of Magnetic Nanoparticles in Polyelectrolyte Brushes. *Adv. Mater.* **2008**, *20*, 4504–4508. doi:10.1002/adma.200801423.
94. Evans, B.A.; Shields, A.R.; Carroll, R.L.; Washburn, S.; Falvo, M.R.; Superfine, R. Magnetically Actuated Nanorod Arrays as Biomimetic Cilia. *Nano Lett* **2007**, *7*, 1428–1434. doi:10.1021/nl070190c.
95. Benkoski, J.J.; Deacon, R.M.; Land, H.B.; Baird, L.M.; Breidenich, J.L.; Srinivasan, R.; Clatterbaugh, G.V.; Keng, P.Y.; Pyun, J. Dipolar assembly of ferromagnetic nanoparticles into magnetically driven artificial cilia. *Soft Matter* **2010**, *6*, 602–609. doi:10.1039/b918215b.
96. Haddour, N.; Chevolot, Y.; Trévisan, M.; Souteyrand, E.; Cloarec, J.P. Use of magnetic field for addressing, grafting onto support and actuating permanent magnetic filaments applied to enhanced biodetection. *J. Mater. Chem.* **2010**, *20*, 8266–8271. doi:10.1039/B920460A.
97. Vilfan, M.; Potočnik, A.; Kavčič, B.; Osterman, N.; Poberaj, I.; Vilfan, A.; Babič, D. Self-assembled artificial cilia. *Proceedings of the National Academy of Sciences* **2010**, *107*, 1844–1847, [https://www.pnas.org/content/107/5/1844.full.pdf]. doi:10.1073/pnas.0906819106.
98. Trévisan, M.; Duval, A.; Moreau, J.; Bartelian, B.; Canva, M.; Monnier, V.; Chevolot, Y.; Cloarec, J.; Souteyrand, E. Assembling, locating, grafting and actuating permanent filaments for validation of Polarimetric Surface Plasmon Resonance Imaging system. *Procedia Engineering* **2011**, *25*, 872 – 875. EurosensorsXXV, doi:https://doi.org/10.1016/j.proeng.2011.12.214.
99. Trévisan, M.; Chevolot, Y.; Monnier, V.; Cloarec, J.P.; Souteyrand, E.; Duval, A.; Moreau, J.; Canva, M. Elaboration and grafting of magnetic bead-chains for detection of anisotropy with polarimetric surface plasmon resonance imaging system. *International Journal of Nanoscience* **2012**, *11*, 1240012. doi:10.1142/S0219581X12400121.
100. Breidenich, J.L.; Wei, M.C.; Clatterbaugh, G.V.; Benkoski, J.J.; Keng, P.Y.; Pyun, J. Controlling length and areal density of artificial cilia through the dipolar assembly of ferromagnetic nanoparticles. *Soft Matter* **2012**, *8*, 5334–5341. doi:10.1039/C2SM25096A.
101. Tokarev, A.; Gu, Y.; Zakharchenko, A.; Trotsenko, O.; Luzinov, I.; Kornev, K.G.; Minko, S. Reconfigurable Anisotropic Coatings via Magnetic Field-Directed Assembly and Translocation of Locking Magnetic Chains. *Advanced Functional Materials* **2014**, *24*, 4738–4745, [https://onlinelibrary.wiley.com/doi/pdf/10.1002/adfm.201303358]. doi:10.1002/adfm.201303358.
102. Sun, L.; Zheng, Y. Bio-inspired artificial cilia with magnetic dynamic properties. *Frontiers of Materials Science* **2015**, *9*, 178. doi:10.1007/s11706-015-0291-y.
103. Hanasoge, S.; Hesketh, P.J.; Alexeev, A. Microfluidic pumping using artificial magnetic cilia. *Microsystems & Nanoengineering* **2018**, *4*, 11. doi:10.1038/s41378-018-0010-9.
104. Vu, A.; Freeman, E.; Qian, X.; Ulbricht, M.; Ranil Wickramasinghe, S. Tailoring and remotely switching performance of ultrafiltration membranes by magneticaly responsive polymer chains. *Membranes* **2020**, *219*, 1–13. doi:10.3390/membranes10090219.
105. Akkilic, N.; Leermakers, F.A.M.; de Vos, W.M. Responsive polymer brushes for controlled nanoparticle exposure. *Nanoscale* **2015**, *7*, 17871–17878. doi:10.1039/C5NR05150A.
106. Fahrni, F.; Prins, M.W.J.; van IJzendoorn, L.J. Micro-fluidic actuation using magnetic artificial cilia. *Lab Chip* **2009**, *9*, 3413–3421. doi:10.1039/B908578E.

107. Babataheri, A.; Roper, M.; Fermigier, M.; Roure, O.D. Tethered fleximags as artificial cilia. *Journal of Fluid Mechanics* **2011**, *678*, 5–13. doi:10.1017/S002211201100005X.
108. Ben, S.; Zhou, T.; Ma, H.; Yao, J.; Ning, Y.; Tian, D.; Liu, K.; Jiang, L. Multifunctional Magnetocontrollable Superwettable-Microcilia Surface for Directional Droplet Manipulation. *Advanced Science* **2019**, *6*, 1900834, [https://onlinelibrary.wiley.com/doi/pdf/10.1002/advs.201900834]. doi:10.1002/advs.201900834.
109. Wei, J.; Song, F.J.; Dobnikar, J. Assembly of Superparamagnetic Filaments in External Field. *Langmuir : the ACS journal of surfaces and colloids* **2016**, *32 36*, 9321–8.
110. Sánchez, P.A.; Pyanzina, E.S.; Novak, E.V.; Cerdà, J.J.; Sintes, T.; Kantorovich, S.S. Magnetic filament brushes: tuning the properties of a magnetoresponsive supracolloidal coating. *Faraday Discuss.* **2016**, *186*, 241–263. doi:10.1039/C5FD00133A.
111. Pyanzina, E.S.; Sánchez, P.A.; Cerdà, J.J.; Sintes, T.; Kantorovich, S.S. Scattering properties and internal structure of magnetic filament brushes. *Soft Matter* **2017**, *13*, 2590–2602. doi:10.1039/C6SM02606K.
112. Sánchez, P.A.; Pyanzina, E.S.; Novak, E.V.; Cerdà, J.J.; Sintes, T.; Kantorovich, S.S. Supramolecular Magnetic Brushes: The Impact of Dipolar Interactions on the Equilibrium Structure. *Macromolecules* **2015**, *48*, 7658–7669, [https://doi.org/10.1021/acs.macromol.5b01086]. PMID: 26538768, doi:10.1021/acs.macromol.5b01086.
113. Rozhkov, D.A.; Pyanzina, E.S.; Novak, E.V.; Cerdà, J.J.; Sintes, T.; Ronti, M.; Sánchez, P.A.; Kantorovich, S.S. Self-assembly of polymer-like structures of magnetic colloids: Langevin dynamics study of basic topologies. *Molecular Simulation* **2018**, *44*, 507–515. doi:10.1080/08927022.2017.1378815.
114. Cerdà, J.J.; Bona-Casas, C.; Cerrato, A.; Novak, E.V.; Pyanzina, E.S.; Sánchez, P.A.; Kantorovich, S.; Sintes, T. Magnetic responsive brushes under flow in strongly confined slits: external field control of brush structure and flowing particle mixture separation. *Soft Matter* **2019**, *15*, 8982–8991. doi:10.1039/C9SM01285K.
115. Cerdà, J.J.; Bona-Casas, C.; Cerrato, A.; Sintes, T.; Massó, J. Colloidal magnetic brushes: influence of the magnetic content and presence of short-range attractive forces in the micro-structure and field response. *Soft Matter* **2021**, *17*, 5780–5791. doi:10.1039/D0SM02006K.
116. Zaben, A.; Kitenbergs, G.; Cebers, A. Deformation of flexible ferromagnetic filaments under a rotating magnetic field. *Journal of Magnetism and Magnetic Materials* **2020**, *499*, 166233. doi:https://doi.org/10.1016/j.jmmm.2019.166233.
117. Belovs, M.; Cēbers, A. Ferromagnetic microswimmer. *Phys Rev E* **2009**, *79*, 051503. doi:10.1103/PhysRevE.79.051503.
118. Hoang, N.; Zhang, N.; Du, H. A dynamic absorber with a soft magnetorheological elastomer for powertrain vibration suppression. *Smart Materials and Structures* **2009**, *18*, 074009. doi:10.1088/0964-1726/18/7/074009.
119. Goubault, C.; Jop, P.; Fermigier, M.; Baudry, J.; Bertrand, E.; Bibette, J. Flexible Magnetic Filaments as Micromechanical Sensors. *Phys. Rev. Lett.* **2003**, *91*, 260802. doi:10.1103/PhysRevLett.91.260802.
120. Liu, J.; Mao, Y.; Ge, J. The magnetic assembly of polymer colloids in a ferrofluid and its display applications. *Nanoscale* **2012**, *4*, 1598–1605. doi:na.
121. Huang, Y.W.; Hu, S.T.; Yang, S.Y.; Horng, H.E.; Hung, J.C.; Hong, C.Y.; Yang, H.C.; Chao, C.H.; Lin, C.F. Tunable diffraction of magnetic fluid films and its potential application in coarse wavelength-division multiplexing. *Opt. Lett.* **2004**, *29*, 1867–1869. doi:10.1364/OL.29.001867.
122. Pirmoradi, F.N.; Jackson, J.K.; Burt, H.M.; Chiao, M. A magnetically controlled MEMS device for drug delivery: design, fabrication, and testing. *Lab Chip* **2011**, *11*, 3072–3080. doi:10.1039/C1LC20438F.
123. Corr, S.A.; Byrne, S.J.; Tekoriute, R.; Meledandri, C.J.; Brougham, D.F.; Lynch, M.; Kerskens, C.; O'Dwyer, L.; Gun'ko, Y.K. Linear Assemblies of Magnetic Nanoparticles as MRI Contrast Agents. *Journal of the American Chemical Society* **2008**, *130*, 4214–4215. doi:10.1021/ja710172z.
124. Wang, H.; Yu, Y.; Sun, Y.; Chen, Q. Magnetic Nanochains: a review. *Nano* **2011**, *06*, 1–17. doi:10.1142/S1793292011002305.
125. Warner, H. R., J. Kinetic Theory and Rheology of Dilute Suspensions of Finitely Extendible Dumbbells. *Industrial and Engineering Chemistry Fundamentals* **1972**, *11*, 379–387. Cited By :385.
126. Weeks, J.D.; Chandler, D.; Andersen, H.C. Role of Repulsive Forces in Determining the Equilibrium Structure of Simple Liquids. *J Chem Phys* **1971**, *54*, 5237–5247. doi:10.1063/1.1674820.
127. Cerdà, J.J.; Ballenegger, V.; Lenz, O.; Holm, C. P3M algorithm for dipolar interactions. *J Chem Phys* **2008**, *129*, 234104. doi:10.1063/1.3000389.
128. Arnold, A.; de Joannis, J.; Holm, C.J. Electrostatics in periodic slab geometries. I. *J. Chem.* **2002**, *117*, 2496.

129. Wang, Z.; Holm, C. Estimate of the cutoff errors in the Ewald summation for dipolar systems. *J. Chem.* **2001**, *115*, 6351.
130. Allen, M.P.; Tildesley, D.J. *Computer Simulation of Liquids*, 1 ed.; Oxford Science Publications, Clarendon Press: Oxford, 1987.
131. Limbach, H.J.; Arnold, A.; Mann, B.A.; Holm, C. ESPResSo – An Extensible Simulation Package for Research on Soft Matter Systems. *Comput Phys Commun* **2006**, *174*, 704–727. doi:10.1016/j.cpc.2005.10.005.
132. Suwa, M.; Tsukahara, S.; Watarai, H. Applications of magnetic and electromagnetic forces in micro-analytical systems. *Lab Chip* **2023**, *23*, 1097–1127.
133. Skjeltorp, A.T. One- and Two-Dimensional Crystallization of Magnetic Holes. *Phys. Rev. Lett.* **1983**, *51*, 2306–2309.
134. Ramos, J.; Klingenberg, D.J.; Hidalgo-Alvarez, R.; de Vicente, J. Steady shear magnetorheology of inverse ferrofluids. *Journal of Rheology* **2011**, *55*, 127–152.